

United States
Department of
Agriculture
Forest Service

**Forest
Products
Laboratory**

Research
Paper
FPL 348
1979

Optimum Fiber Distribution in Singlewall Corrugated Fiberboard

Abstract

Determining optimum distribution of fiber through rational design of corrugated fiberboard could result in significant reductions in fiber required to meet end-use conditions, with subsequent reductions in price pressure and extension of the softwood timber supply.

A theory of thin plates under large deformations is developed that is both kinematically and physically nonlinear. This theory is used to analyze the strength of a singlewall fiberboard element which is modeled as a composite plate structure. Either an elastic-type instability or a compression failure mode is allowed. The results of this analysis are used to explain how to adjust facing and corrugating medium thicknesses to maximize the edgewise compression strength per board weight.

Keywords : Buckling, compression, corrugated, design, elasticity, fiberboard, model, nonlinear, optimize, plates, strength.

OPTIMUM FIBER DISTRIBUTION IN SINGLEWALL CORRUGATED FIBERBOARD

By

MILLARD W. JOHNSON, JR.^{1/}

THOMAS J. URBANIK, Research General Engineer

WILLIAM E. DENNISTON^{1/}

Forest Products Laboratory,^{2/} Forest Service
U.S. Department of Agriculture

Introduction

In the design of fiberboard containers, one of the basic problems is to distribute the material between facings and corrugating medium to maximize top-to-bottom compression strength. Both short-column edgewise compressive strength and board stiffness contribute to the overall strength, and have been investigated.

One of the earliest theories of efficient design, prepared by Kellicutt (4),^{3/} was to maximize strength by maximizing the board stiffness. Kellicutt advocated locating most of the material in the facings to maximize the moment of inertia and the bending stiffness. He also developed a formula for calculating the moment of inertia for a corrugated cross section.

The theory developed by McKee, Gander, and Wachuta (7) accounts for both short-column strength and board stiffness. It is shown that the optimal design strikes a balance between these two considerations, with short-column strength playing an important role because of the nonuniform axial stress distribution across the fiberboard panel. Their theory is based on the theory for the buckling of thin plates modified empirically to match experimental data. The short-column strength, which enters the

^{1/} Professor and graduate student, respectively, Dept. of Engineering Mechanics, University of Wisconsin-Madison.

^{2/} Maintained at Madison, Wis., in cooperation with the University of Wisconsin.

^{3/} Underlined numbers in parentheses refer to literature cited at the end of this report.

formula for overall strength, is obtained by direct experimental measurement.

Moody (8) provided an analytical method for determining the short-column strength based on local buckling of the fiberboard elements. His theory agrees reasonably well with certain experimental data. It uses results from design procedures developed for airplane structures based on the fundamental work of Cox (1). The theory allows the use of nonlinear stress-strain data. However, the method of calculation does not lend itself to the analysis of a large number of parameter values.

Zahn (12) has reconsidered the foundations of the local buckling theory and provided a computer program to analyze a large number of parameter values. This analysis is restricted to linear stress-strain relationships. Both corrugating medium and facings must have the same elastic properties. The theories of both Moody and Zahn cannot accommodate an arbitrary takeup factor in the corrugated fiberboard except by an arbitrary approximation of the geometry. Zahn's theory allows a mode of buckling with nodal lines diagonal to the compressive load. This mode is not included in Moody's analysis or in that of this paper. Some comparison of Zahn's method with that developed here is made in the section "Numerical Results and Comparison"

The purpose of this paper is twofold. One is to formulate a theory for short-column strength of the local buckling type which allows nonlinear elastic behavior, different elastic properties of medium and facing, and an arbitrary takeup factor, and which provides computer program which can be easily used to generate results for a large number of parameter values. The mathematical analyses is summarized and an iterative method for the solution of the buckling equation discussed. An empirical formula is used to fit the nonlinear compressive stress-strain data, and numerical results are compared with experimental data.

Our second aim is to examine the foundations of the nonlinear theory of plates on which our buckling theory is based. A theory for the large deformation of plates is developed which allows both kinematical and physical nonlinearity as well as anisotropic elastic properties. We know of no other theory with this generality which is needed for a complete description of paper behavior. While this theory is not used here in its full generality, it is presented as a basis for future contemplated theoretical and experimental research. An elastic stability theory is developed here and used to analyze the strength of a short fiberboard element modeled as a composite plate structure.

Buckling Model Development

If an element of corrugated fiberboard is under a uniform compressive stress applied parallel to the corrugations, it may fail due to local elastic buckling. This mode of buckling is characterized by a large number of lateral deflection half-waves in the direction of the load. Their length scale is that of the microstructure. We note that, before local buckling can take place, the material may fail due to the ultimate compressive stress being reached.

To develop the mathematical model for local buckling, the corrugated fiberboard is represented as a composite plate structure (fig. 1). The nonlinear theory of plates is used for each element and the solution of the governing differential equations for local buckling is discussed in the section "Local Instability" The most serious assumptions in the theory are that the plates are isotropic and that linear stress-strain equations can be used with an additional ad hoc assumption which substitutes the tangent modulus for Young's modulus.

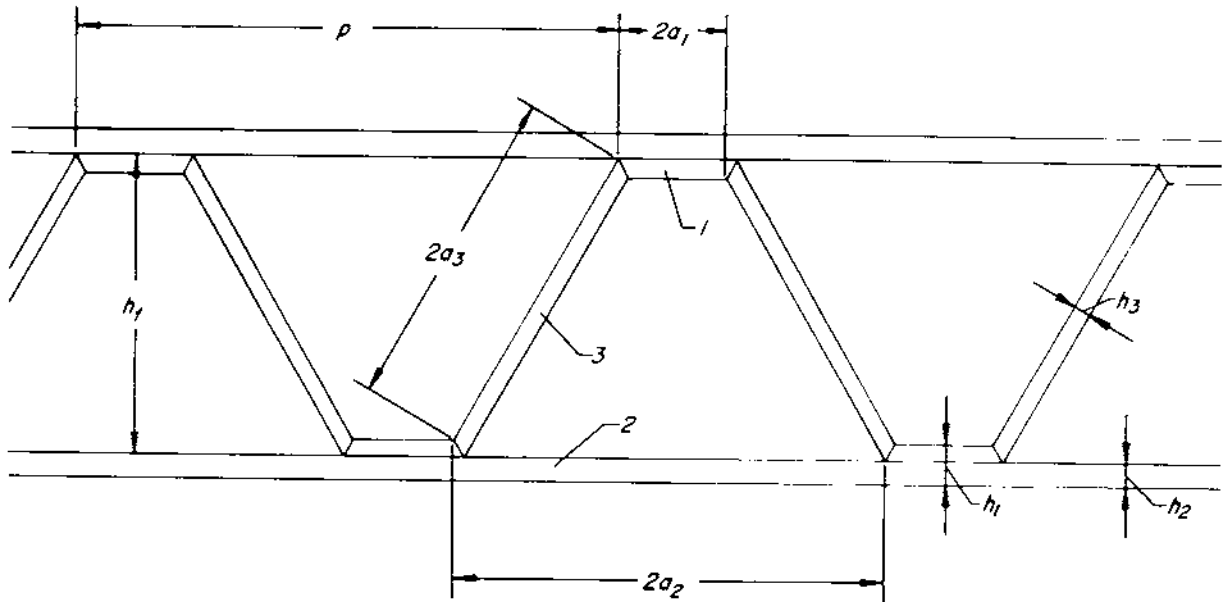
A buckling equation is obtained by satisfying boundary conditions that require that the plate elements are rigidly fastened and that the junctures be in moment equilibrium. The buckling equation is given by (3.3.13) in the form:

$$K_1 + K_2 + K_3 = 0 \quad (2.1.1)$$

where K_i ($i = 1,2,3$) are plate stiffness coefficients for each plate element given by (3.3.16):

$$K_i = \frac{E_i t_i^2 \sqrt{(1-\nu_i^2)\sigma_i/E_i}}{\alpha_i \tan(\alpha_i b_i) + \beta_i \tanh(\beta_i b_i)} \quad (2.1.2)$$

where α_i and β_i are defined by (3.3.15). The subscript refers to the plate element (fig. 1), σ_i is the compressive stress at buckling, E_i the tangent modulus, $t_i L$ plate element thickness, $b_i L$ plate width, and L the



M 148 072

Figure 1.--Structural model for singlewall corrugated fiberboard.

length of the sheet in the direction of the load. In eqs. (3.3.15) n is the number of half-wave buckles.

The dimensional parameters in fig. 1 can be derived from the more commonly understood corrugated fiberboard geometry. We have

$$h_1 = h_2 + h_3$$

where

h_2 = facing thickness

h_3 = corrugating medium thickness.

From the makeup factor, TF, and the flutes per foot, F, we obtain the effective spacing between flute tips as

$$p \text{ (in.)} = 12/F$$

and the half-width of each plate element as

$$a_1 = \frac{p^2 (TF^2 - 1) - 4(h_f - h_3)^2}{8 p (TF - 1)}$$

$$a_2 = p/2 - a_1$$

$$a_3 = p \times TF/4 - a_1$$

where

$$h_f = \text{flute height.}$$

It is found that the available stress-strain data for paper under edge-wise compression can be fit quite accurately up to the ultimate stress with the empirical formula:

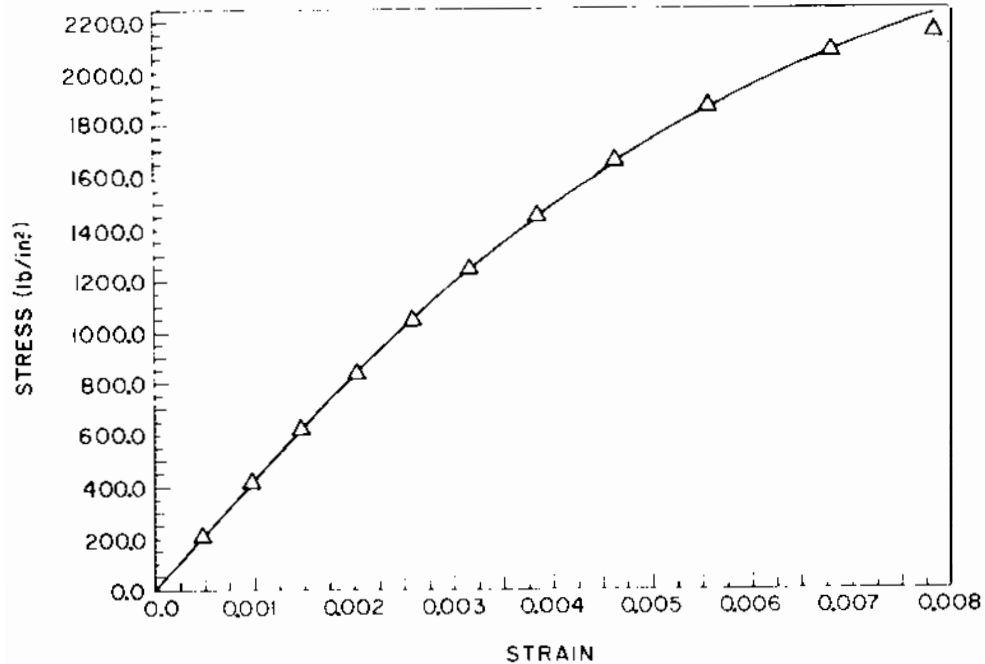
$$\sigma(\varepsilon) = c_1 \tanh(c_2 \varepsilon) + c_3 \varepsilon \quad (2.1.3)$$

Here σ and ε are axial engineering stress and strain derived from the applied load per undeformed area and the displacement per initial length. σ is identical with N_{11}/h and ε with ε_1 in the stress-strain relation (3.1.25). Details on how coefficients c_i are determined to fit the data

are given in "Empirical Stress-Strain Formula." A Curve of form of eq. (2.1.3) is fitted to data for facing and corrugating medium (fig. 2). The tangent modulus is given by

$$E(\varepsilon) = \sigma' = c_1 c_2 / \cosh^2(c_2 \varepsilon) + c_3 \quad (2.1.4)$$

Since buckling usually occurs when the strain is greater than the proportional limit, the stress σ_i and modulus E_i in (2.1.2) are taken to be



M148 073

Figure 2. --An empirically derived curve
 $\sigma(\epsilon) = 1,842 \tanh (196.2\epsilon) + 70,009 \epsilon \text{ lb/in.}^2$.

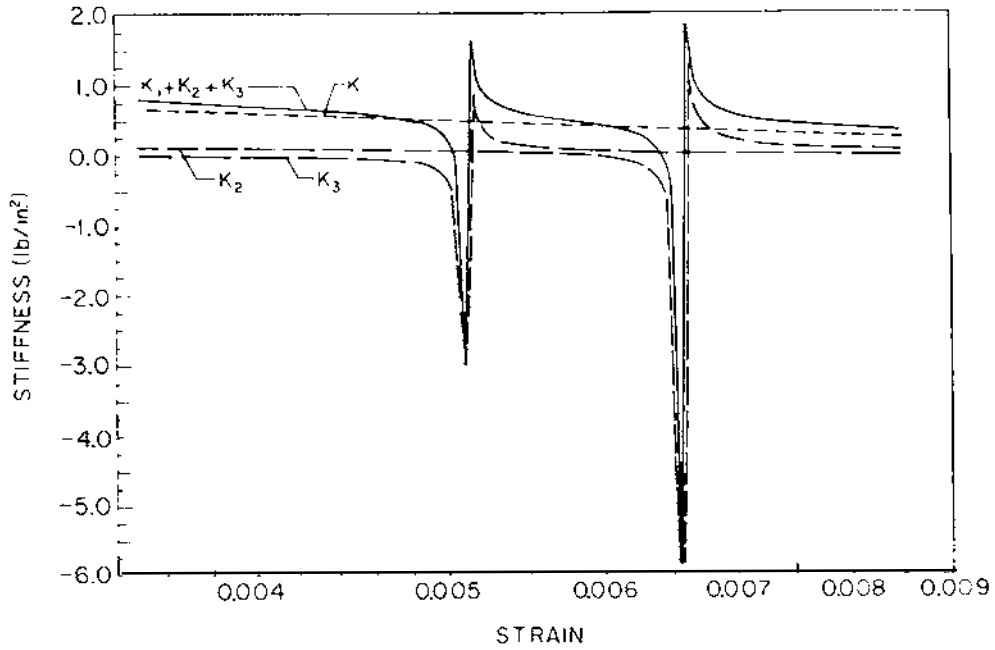
given by eqs. (2.1.3) and (2.1.4) using coefficient values appropriate to either facing or medium. With stress and modulus given in terms of strain by (2.1.3) and (2.1.4), we see that (2.1.1) and (2.1.2) are equations for the strain ϵ at buckling. For typical fiberboard properties, figure 3 shows the stiffness coefficients K_1 for the three plate elements

(fig. 1) and their sum as functions of strain ϵ . The number of half-waves is taken as $n = 7$.^{4/} The smallest zero of the sum corresponds to the primary mode of buckling (fig. 4). The higher zeros correspond to modes in which the plate elements undergo wavier deformations. The primary mode that has the smallest strain is of interest. In addition, n , the number of half-waves, must be chosen to minimize further the primary buckling strain.

The analytical solution of eq. (2.1.1) must be arrived at by a method of successive approximation. It is found that the following algorithm converges rapidly to an accurate buckling strain. If the buckling is initiated by element 2, start by solving (2.1.1) for K_2 :

$$K_2 = - (K_1 + K_3)$$

^{4/} Additional input to (2.1.1) are at $L = 1.0$, $t_1 = 0.0194$, $t_2 = 0.012$, $t_3 = 0.0074$, $b_1 = 0.0537$, $b_2 = 0.280$, $b_3 = 0.206$, and $v_1 = v_2 = v_3 = 0.268$.



M 148 077

Figure 3.--Stiffness coefficients for A-flute construction with 36 flutes per foot, 0.18-inch flute height, 1.56 takeup factor, and stress-strain curves for both components given by figure 2. Facing thickness is 0.012 inch; medium thickness is 0.0074 inch.

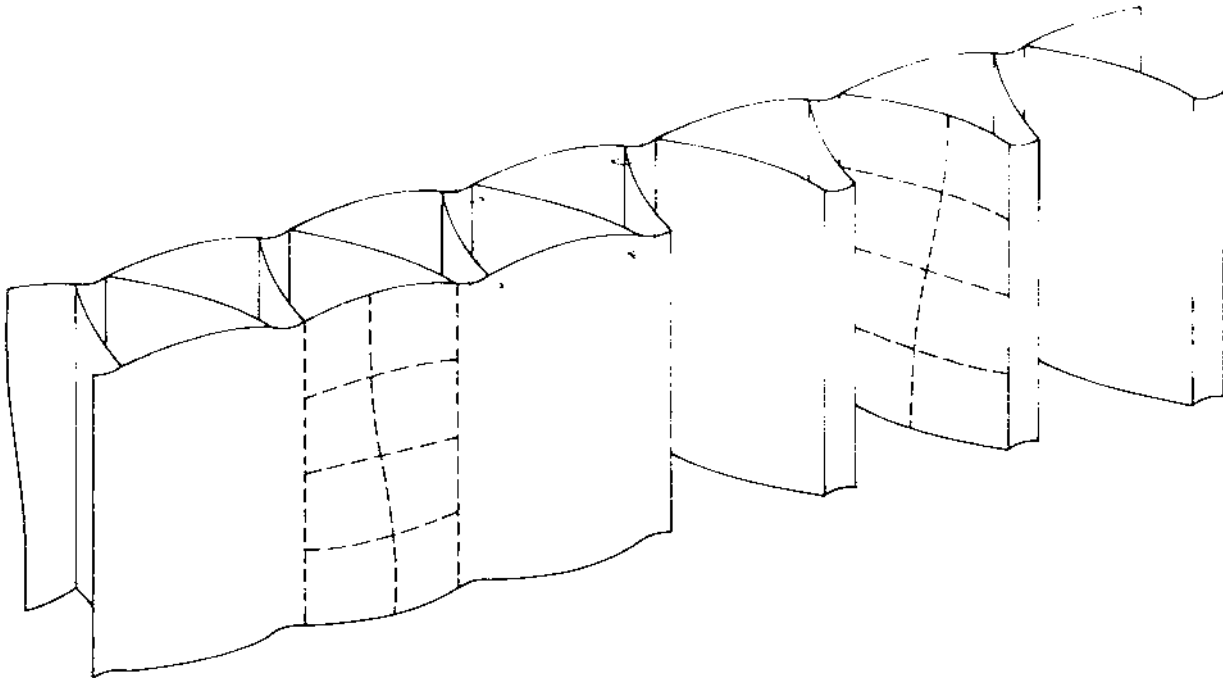


Figure 4.--Primary buckling mode.

M148074

Then, solve this equation for $\tan(\alpha_2 b_2)$

$$\tan(\alpha_2 b_2) = -\frac{\beta_2}{\alpha_2} \tanh(\beta_2 b_2) - \frac{E_2 t_2^2 \sqrt{(1-\nu_2^2)} \sigma_2 / E_2}{\alpha_2 (K_1 + K_3)} \quad (2.1.5)$$

Next, define

$$\gamma = \frac{\sqrt{12(1-\nu_2^2)} \sigma_2 / E_2}{n\pi t_2} \quad (2.1.6)$$

Then, (3.3.15) becomes

$$\alpha_2 = n\pi \sqrt{\gamma-1} \quad , \quad \beta_2 = n\pi \sqrt{\gamma+1} \quad (2.1.7)$$

Introduce (2.1.7) in (2.1.5) and invert the tangent function. After some manipulation, we get

$$\gamma = 1 + \frac{1}{(n\pi b_2)^2} \left\{ \pi - \arctan \left[\sqrt{\frac{\gamma+1}{\gamma-1}} \tanh(n\pi b_2 \sqrt{\gamma+1}) \right] + \frac{E_2 t_2^3 \gamma}{\sqrt{12(\gamma-1)} (K_1 + K_3)} \right\}^2 \quad (2.1.8)$$

Solve (2.1.8) by iteration, the current estimate for γ going in the right side to generate a new estimate for γ . The steps in the iteration are

1. Initialize n as $n \sim L/b$ where L is the length and b the width of the plate.
2. Initialize $\gamma = \gamma_1$ as slightly greater than 1.

3. From eqs. (2.1.3), (2.1.4), and (2.1.6),

$$\frac{c_1 \tanh(c_2 \varepsilon) + c_2 \varepsilon}{c_1 c_2 \operatorname{sech}^2(c_2 \varepsilon) + c_3} = \frac{n^2 \pi^2 t_2^2}{12(1-\nu_2^2)} \gamma_1^2$$

This equation is solved by Newton's method to give an estimate of the buckling strain ε .

4. Compute $\sigma_1(\varepsilon)$, $s_3(\varepsilon)$, $E_1(\varepsilon)$, $E_3(\varepsilon)$ from (2.1.3) and (2.1.4). Compute α_1 , α_3 , β_1 , β_3 from (3.3.15). Compute K_1 and K_3 with (2.1.2).
5. Compute right side of (2.1.8) for new estimate $\gamma = \gamma_2$.
6. If

$$\left| \frac{\gamma_2}{\gamma_1} - 1 \right| < \text{error bound}$$

go to step 7. Otherwise go to step 3.

7. Increase n by 1. Go to step 3. n is incremented until the minimum buckling strain ε is reached.

To speed convergence, an overrelaxation scheme is used in the form

$$\text{new } \gamma = \alpha \gamma_1 + (1-\alpha) \gamma_2$$

where $0 < \alpha < 1$ is a convergence factor.

Both eq. (2.1.8) and the corresponding one assuming buckling is initiated in element 3 are used in the program. We have found that this algorithm makes possible an efficient computer solution for economically reducing the analysis to a design curve.

An Empirical Stress-Strain Formula

An equation of the form

$$\sigma(\epsilon) = c_1 \tanh(c_2 \epsilon) + c_3 \epsilon$$

has been found to provide a good fit to the experimental stress-strain data digitized from a load-deformation curve for a paperboard specimen in edgewise compression. If there are n data points (σ_i, ϵ_i) that define an experimentally produced curve, the coefficients to the equation may be initialized and then adjusted to improve the accuracy of fit.

From the equation for $\sigma(\epsilon)$ and its derivative

$$\sigma'(\epsilon) = \frac{c_1 c_2}{\cosh^2(c_2 \epsilon)} + c_3$$

as ϵ approaches infinity, the limiting value for $\sigma(\epsilon)$ becomes

$$\sigma_n + c_1 + c_3 \epsilon_n$$

which can be used to estimate c_1 when c_3 is known.

For $\sigma'(\epsilon)$ the limit is c_3 . At a stress near the ultimate level the limit for $\sigma(\epsilon)$ is nearly satisfied; from its tangent slope calculate

$$c_3 = \frac{\sigma_n - \sigma_{n-1}}{\epsilon_n - \epsilon_{n-1}}$$

Now at ϵ equal to zero

$$\sigma'(0) = c_1 c_2 + c_3$$

from which an estimate may be obtained for

$$c_1 c_2 = \frac{\sigma_1}{\epsilon_1} - c_3$$

This is used to calculate c_2 after c_1 and c_3 have been calculated above.

With a computer program the coefficients may be refined to provide a more closely fit equation. Generate the array

<u>u</u>	<u>v</u>	<u>w</u>
$(1 - e)c_1$	$(1 - e)c_2$	$(1 - e)c_3$
c_1	c_2	c_3
$(1 + e)c_1$	$(1 + e)c_2$	$(1 + e)c_3$

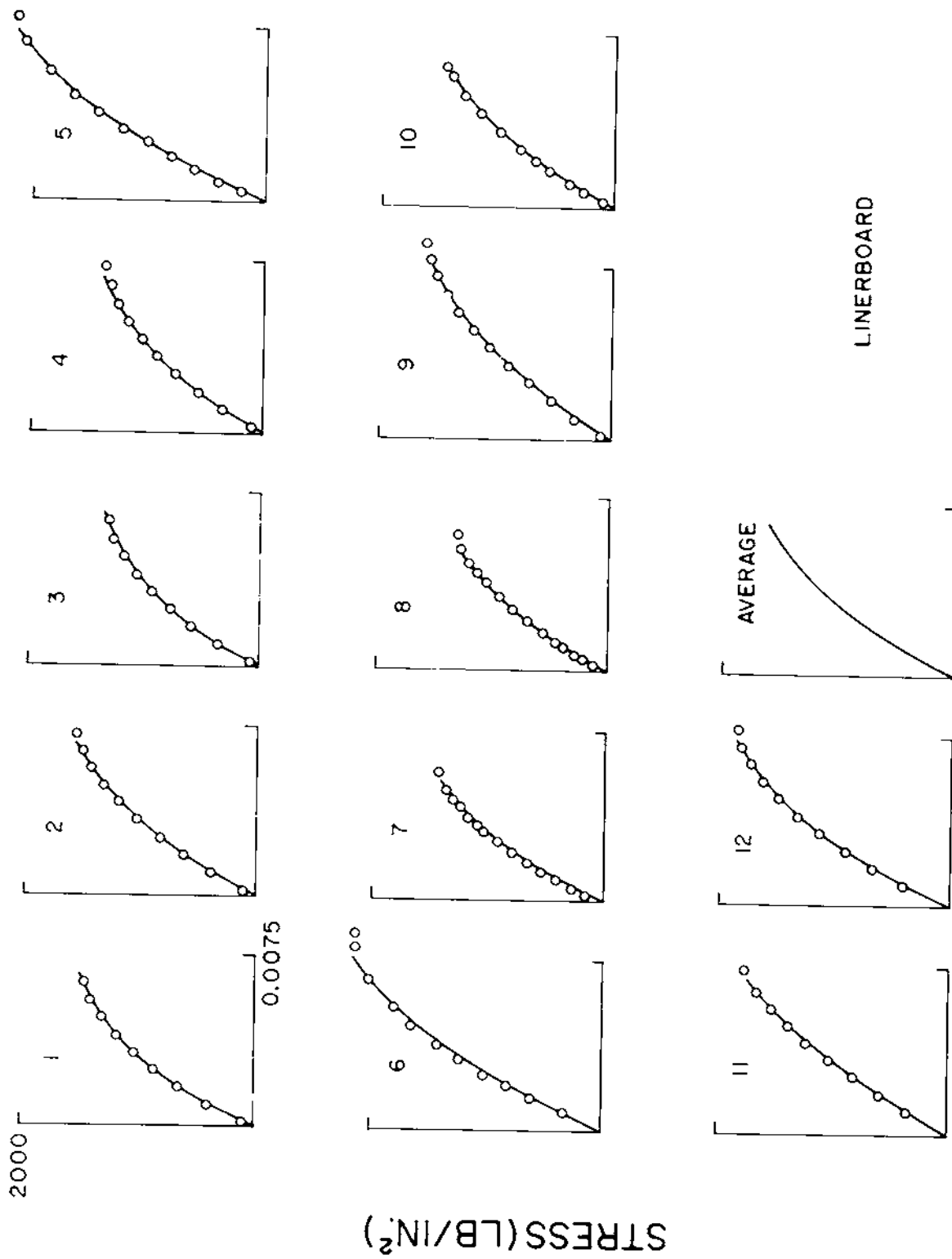
from some small value e and the initialized coefficients. Select one coefficient from each column, that is c_u , c_v , and c_w (27 possible com-

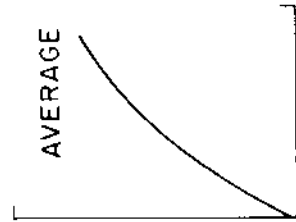
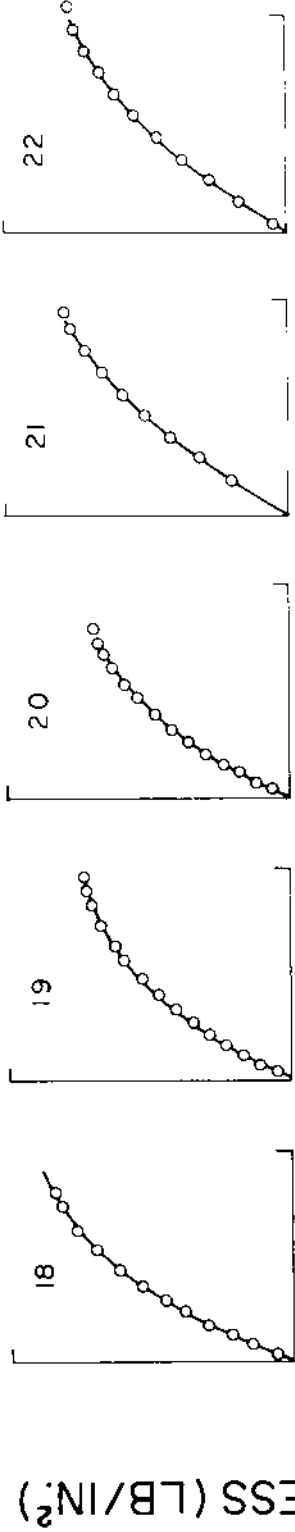
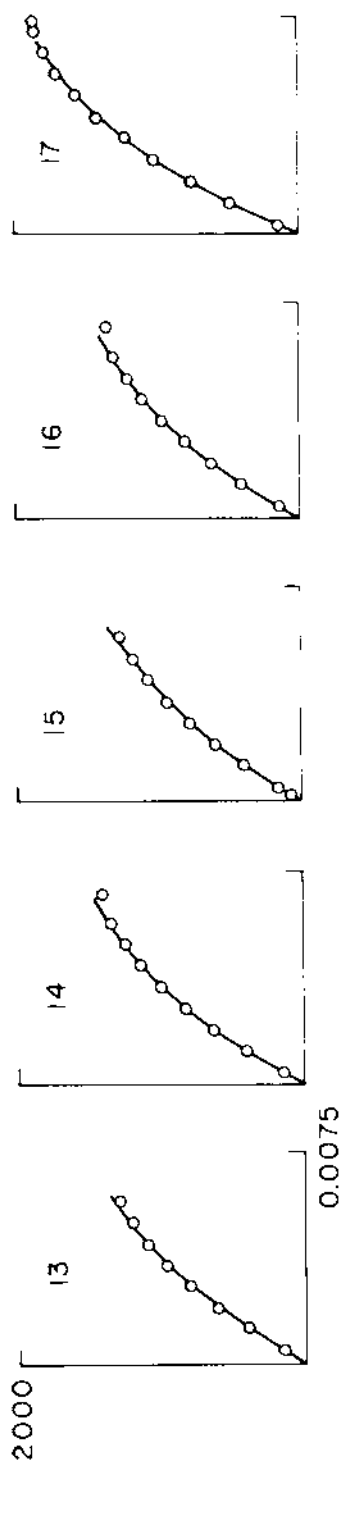
binations), and compare the fit equation to the original data. Define the measure of fit as the average relative difference between the stress data and the functional evaluations at the strain data,

$$M_f = \frac{1}{n} \sum_{i=1}^n \left| \frac{\sigma_i - \sigma(\epsilon_i)}{\sigma_i} \right|$$

Then let the coefficients c_1 , c_2 , and c_3 take on the new values of c_u , c_v , and c_w that minimize M_f .

A load-deflection curve for a 42-pound linerboard in the cross-machine direction was plotted via an autograph recorder (fig. 2). Eleven points were read from the curve, adjusted to appropriate units, and used to determine the coefficients. The fit was accepted with an average relative difference of 1.02 percent. This curve appears as number 5 in figure 5. The other curves in Figure 5 are determined in the same manner. Table 1 gives the coefficients and the ultimate stresses for these curves.



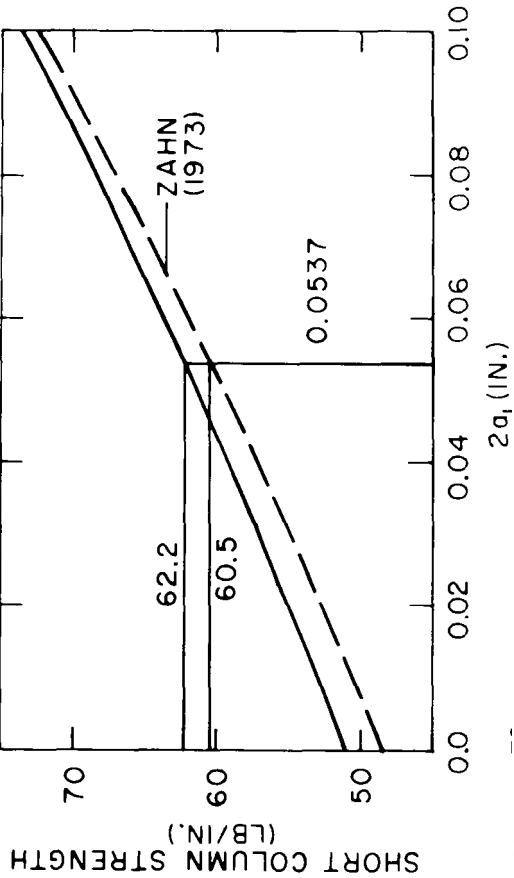


CORRUGATING MEDIUM

STRAIN (IN./IN.)

M 148 076

Figure 5.--Plots of eq. (2.1.3) fit to the edgewise compression data for linerboard and corrugating medium. An average curve is given for each component.



M 148 079

Figure 6.--Comparison between this analysis and Zahn's 1973 analysis (12) dependent on the size of the flute tip. The calculations assume 36 flutes per foot, 1.56 takeup factor, 0.012-inch facing thickness, and 0.0074-inch medium thickness. The stress-strain curves for both components are given by figure 2.

Table 1.--Equation (2.1.3) coefficients to the stress-strain data (fig. 5)

Curve number (fig. 5)	C_1	C_2	C_3	Ultimate stress, σ_u Lb/in. ²
Linerboard				
1	1,040.	332.1	74,180	1,510
2	1,002.	268.3	91,140	1,590
3	922.7	332.1	65,810	1,340
4	889.0	268.3	80,860	1,410
5	1,842.	196.2	70,009	2,153
6	1,374.	226.2	116,700	2,170
7	1,031.	300.3	87,230	1,410
8	896.4	265.7	94,050	1,320
9	1,019.	205.8	84,180	1,610
10	823.1	291.4	113,800	1,450
11	906.3	230.6	137,200	1,770
12	1,726.	205.5	39,870	1,860
Average ^{1/}	1,123.	251.8	87,920	1,630
Corrugating medium				
13	574.8	326.1	139,300	1,420
14	783.3	106.4	108,400	1,490
15	559.5	326.1	135,600	1,380
16	762.4	306.4	105,500	1,450
17	1,423.	241.9	76,380	1,859
18	1,420.	295.1	57,060	1,775
19	1,151.	297.5	48,370	1,460
20	917.2	320.3	88,140	1,370
21	1,061.	217.8	89,750	1,570
22	1,187.	206.8	60,000	1,510
Average ^{1/}	983.9	276.4	90,850	1,530

^{1/} Average coefficients for n curves are found to satisfy the following: $\text{av. } C_1 = (\sum C_1)/n$; $\text{av. } C_2 = (\sum C_2)/n$; $\text{av. } C_3 = (\sum C_3)/n$; $\text{av. } \sigma_u = (\sum \sigma_u)/n$.

Table 2.--Edgewise compression strength analysis compared to observations

Flute size	Flutes per foot	Flute height	Takeup factor	Thickness			Stress-strain curve number (fig. 5)		Edgewise compression strength		Difference	Predicted failure ^{1/}	
				Facing	Medium	Measurement method	Facing	Medium	Observed	Predicted		Type	Component
A (6)	36	0.177	1.55	0.0118	0.0073	Stylus	1	13		44.6		B	F
							1	14		44.6		B	M
						(10)	2	13		46.7		B	M
							2	14		<u>44.3</u>		B	M
									45.8	<u>2/</u> 45.0	-1.75		
A (6)	36	.174	1.55	.0133	.0075	TAPPI	3	15		48.8		B	F
							3	16		46.5		B	M
							4	15		49.7		B	M
							4	16		<u>46.5</u>		B	M
									45.8	47.9	4.59		
A (6)	36	.180	1.55	.0106	.0080	Stylus	5	17		56.9		B	M
							5	18		52.3		B	M
							6	17		56.0		B	M
							6	18		<u>51.5</u>		B	M
									53.8	54.1	0.558		
A (5)	36	.178	1.55	.0078	.0084	Stylus	7	19		29.6		B	F
							7	20		29.4		B	F
							8	19		30.0		B	F
							8	20		<u>28.8</u>		B	F
									31.4	29.2	-7.00		
A (5)	36	.178	1.55	.0185	.0084	Stylus	9	19		59.8		B	M
							9	20		63.7		B	M
							10	19		63.5		B	M
							10	20		<u>67.3</u>		B	M
									65.5	63.6	-2.90		
A	36	.177	1.53	.0108	.0080	Stylus	11	21		51.2		B	M
							11	22		49.0		B	F
							12	21		49.1		B	F
							12	22		<u>48.1</u>		B	F
									45.6	<u>49.3</u>	8.19		
B	50	.0941	1.36	.0108	.0080	Stylus	11	21		55.3		C	M
							11	22		54.2		C	F
							12	21		56.0		C	M
							12	22		<u>56.4</u>		C	M
									48.5	55.4	14.3		
C	42	.142	1.46	.0108	.0080	Stylus	11	21		56.5		C	M
							11	22		55.3		C	F
							12	21		52.8		B	F
							12	22		<u>51.7</u>		B	F
									46.4	54.1	16.6		

^{1/} B, buckling; C, compression; F, facing; M, medium.

^{2/} Average of 4 predictions.

Numerical Results and Comparison with Experimental Data

The buckling strain solved from (2.1.1) yields the stress in each element from the respective stress-strain curve. These stresses distributed over the combined board cross-sectional area define the failure load per unit length of board and predict the specimen edgewise compressive strength.

Comparisons between predicted and experimentally determined edgewise compression strengths are presented in table 2. Some of the experimental values are taken from data collected for other FPL investigations (5,6). The remaining data are from tests performed for this study. The reported observations are average short-column strengths. All available FPL short-column data were used where the paper stress-strain data were also available. The predictions are derived from unpublished load-deformation curves for the component papers of the short-column specimens. Eq. (2.1.3) is plotted for each fit to the paper data (fig. 5). Two representative curves are given for each paper, one with a maximum load above and one below the average maximum load.

All materials were preconditioned at 80° F and 30 percent relative humidity (RH) and conditioned at 73° F and 50 percent RH prior to testing at 73° F and 50 percent RH. The paper components were tested for edgewise compression in the cross-machine direction utilizing the support device described by Jackson (3). The rate of strain was 0.01504 inch/inch/minute. The short-column strength values were then adjusted to the components' strain rates according to Moody and Koning (9). The construction of these specimens is described in TAPPI Standard T811 (11).

The predicted location of failure and either the buckling or compression mode are identified. Compression failure is defined as occurring when the applied load produces a paper stress equal to a component's ultimate stress before buckling can occur. One observes that the prediction is sensitive to the stress-strain curve shapes. An average prediction is thus derived from the permutations among curve replicates.

The A flute data shows the theory to agree well with experiments. A buckling model unadjusted to empirical observations would normally yield high predictions. It is difficult to design a model that accomodates all possible deformations. It appears that our use of the tangent modulus theory and the assumed isotropic behavior compensates for this effect.

For the B and C flute data compression failure is usually predicted at the ultimate stress for one of the components. The compression stress-strain data were produced with the paper restrained against lateral

deflections. The accuracy of this procedure was checked against tensile data. The stress-strain curves in opposite directions were found to agree (3). It is logical to expect a plate element between flute tips, not fully restrained against lateral deflections, to fail in compression at a stress below the measured ultimate. The B and C flute data support this. It remains to be investigated how to best adjust the theory to utilize the stress-strain relationship for predicting compression failure with greater accuracy.

One can compare our analysis to Zahn's by altering the corrugated fiberboard geometry. In figure 1, let h_f be dependent on $2a_1$, h_3 , p , and TF . Then let $2a_1$ vary from zero to some small length. The predicted short-column strength varies with a changing geometry (fig. 6). The point at $2a_1$ equal to 0.0537 inch is compatible with nominal A flute. Zahn's analysis assumes a triangular truss-core shape such that $2a_1$ equals zero. An approximation to Zahn's geometry can be obtained as follows: Let $2a_1$ equal zero and reduce $2a_2$ by $2a_1$. Calculate the buckling stress for this new structure. From this stress) determine the edgewise compression strength for the stress distributed over the original geometry. Zahn's method yields a consistently lower strength prediction than ours. The reason for this is that in the limit as a_1 approaches zero our mode shape does not approach the correct mode shape used by Zahn for the triangular truss-core. Zahn's program apparently is not compatible with the structure for calculating accurate buckling loads for fiberboard structures with takeup factors that result in a $2a_1$ greater than zero.

From the short-column strength prediction, the effect of distributing fiber through the board may be examined. Figure 7 results from successively solving eq. (2.1.1) over an array of facing and medium thickness combinations. Solid line contours of equal short-column strength are produced via an interpolating scheme that locates all the facing and medium pairs that produce equal edgewise compression strengths. Likewise, the dashed lines define the board weights from the combined paper weights and the takeup factor. In this case a 0.012-inch paper was assumed to weigh 42 pounds per thousand square feet and proportional equivalents were applied to other thicknesses.

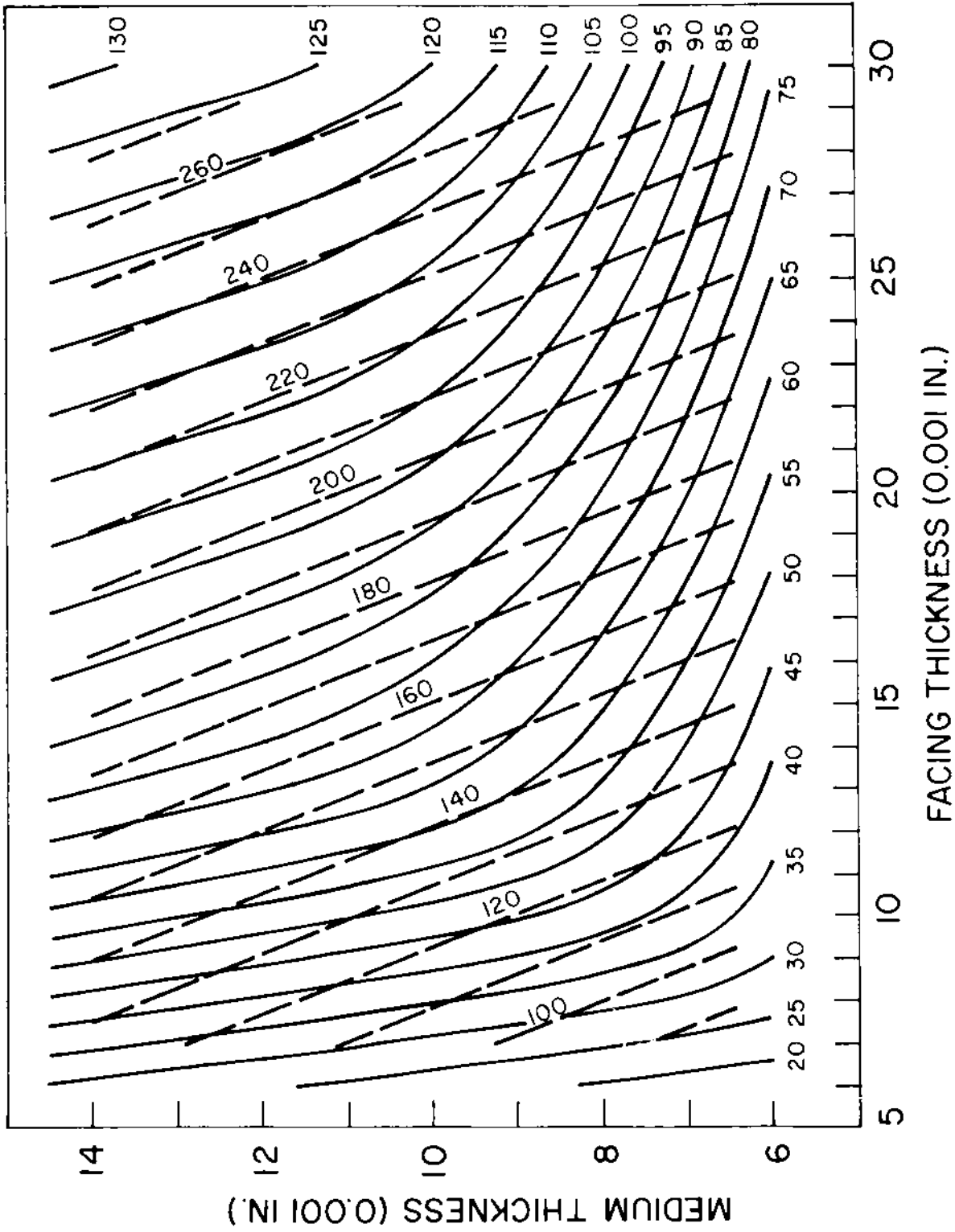
As there is yet little basis for selecting a stress-strain curve shape dependent upon paper thickness and content, average stress-strain curves were determined from the stress-strain data. The average linerboard curve and average medium curve are shown (fig. 5); their coefficients are given in table 1. These representative curves were used in all the calculations to represent the facing and medium material over all thicknesses. Additionally, the structure analyzed was A flute with the same geometry as that used to produce figure 3.

Figure 7 identifies regions for distributing fiber most efficiently by the relative slopes between strength and weight contours. As all example, given the board with a 0.018-inch facing and a 0.00762-inch medium, the short-column strength is read at 65 pounds per inch (lb/in.). For a desired strength increase of 5 lb/in., the facing thickness may be maintained with the medium thickness increased to 0.00817 or the medium may be held constant while the facing is increased to 0.0198. Both alternatives yield a 70 lb/in. short-column. However, the combined board weight increases from 168 to 171 pounds by adding fiber to the medium and to 180 pounds by adding fiber to the facings. It is thus more efficient to add material to the medium for a board from the region of the curve with strength contours shallower than the weight contours.

Where the strength contours are steeper, the board strength is most efficiently improved by adding fiber to the facings. This becomes apparent by moving from a 133-pound board with 0.00966-inch facings and a 0.012-inch medium to either a 145-pound board with the same facings and a 0.0142-inch medium or a 130-pound board with 0.0104-inch facings and the same medium. In either case, the short-column strength increases from 50 to 55 lb/in.

Where the strength contours become tangent to the weight contours, the optimum design is achieved. The facings and medium are balanced for a desired strength with minimum fiber.

Figure 7.--Edgewise compression strength (lb/in., solid lines) and combined board weight (lb/1,000 ft², dashed lines) over an array of facing and corrugating medium combinations. The stress-strain relationship for the facing and medium is given by the average curves in figure 5. The construction is A flute with 36 flutes per foot, 0.18-inch flute height, and a 1.56 takeup factor.



M148 078 Thickness is determined according to the FPL stylus method (10).

Equations For Large Deflection of Anisotropic Plates

We denote Cartesian material and spatial coordinates by x_i and \mathbf{x}_i . The x_i locate the position of a material particle in the reference state while ξ_i locate position in the current configuration. Denote the material (or Piola) stress tensor (2) by P . Component P_{ij} represents force per unit reference area acting in the j -direction associated with a reference face perpendicular to the i -direction.

Because tensor P is associated with areas and directions in the reference configuration, it is a convenient measure of stress to use for the development of a large deformation theory of plates. For no body forces, the equations of equilibrium can be written as (2)

$$\frac{\partial P_{ij}}{\partial x_i} = 0 \quad (3.1.1)$$

Note that x_i are material coordinates and that eqs. (3.1.1) are exact; they contain no approximations for small deformation. Define force and moment resultants by:

$$N_{ij} = \int_{-h/2}^{h/2} P_{ij} dx_3, \quad M_{ij} = \int_{-h/2}^{h/2} P_{ij} x_3 dx_3 \quad (3.1.2)$$

where the integrations are taken over the thickness of the plate and h is thickness of the plate in the reference configuration.

We assume that

$$\left. \begin{aligned} P_{31}(h/2) &= P_{31}(-h/2) = 0 \\ P_{32}(h/2) &= P_{32}(-h/2) = 0 \\ P_{33}(h/2) - P_{33}(-h/2) &= q(x_1, x_2) \end{aligned} \right\} (3.1.3)$$

Integration of eqs. (3.1.1) and use of conditions (3.1.3) yields:

$$\left. \begin{aligned} \frac{\partial N_{11}}{\partial x_1} + \frac{\partial N_{21}}{\partial x_2} &= 0 \\ \frac{\partial N_{12}}{\partial x_1} + \frac{\partial N_{22}}{\partial x_2} &= 0 \\ \frac{\partial N_{13}}{\partial x_1} + \frac{\partial N_{23}}{\partial x_2} + q &= 0 \end{aligned} \right\} (3.3.4)$$

Next, multiply the first two equations of (3.1.1) by x_3 and integrate.

$$\left. \begin{aligned} \frac{\partial M_{11}}{\partial x_1} + \frac{\partial M_{21}}{\partial x_2} &= N_{31} \\ \frac{\partial M_{12}}{\partial x_1} + \frac{\partial M_{22}}{\partial x_2} &= N_{32} \end{aligned} \right\} (3.1.5)$$

Eqs. (3.1.4) are the equations of force equilibrium and (3.1.5) the equations of moment equilibrium of a plate element.

We formulate the stress-strain relations through use of the work principle:

$$\dot{H} = P_{ki} \dot{F}_{ik} \quad (3.1.6)$$

where H is the strain energy density, $F_{ij} = \partial \xi_i / \partial x_j$ components of the deformation gradient tensor and the dot indicates the material time derivative. The integrated form of (3.1.6) is:

$$\dot{\mathcal{L}} = \int_{-h/2}^{h/2} P_{ki} \dot{F}_{ik} dx_3 \quad (3.1.7)$$

where $\mathcal{L} = \int_{-h/2}^{h/2} H dx_3$ is the plate strain energy density.

To proceed further we make the usual assumptions for a thin plate concerning the form of the displacement components, $u_i = \xi_i - x_i$. We set

$$\left. \begin{aligned} u_1 &= U_1(x_1, x_2) - x_3 \frac{\partial w(x_1, x_2)}{\partial x_1} \\ u_2 &= U_2(x_1, x_2) - x_3 \frac{\partial w(x_1, x_2)}{\partial x_2} \\ u_3 &= w(x_1, x_2) \end{aligned} \right\} (3.1.8)$$

where U_1 , U_2 , and w are components of middle surface displacement. The components of finite strain are given by

$$2 E_{ij} = \frac{\partial u_i}{\partial x_j} + \frac{\partial u_j}{\partial x_i} + \frac{\partial u_k}{\partial x_i} \frac{\partial u_k}{\partial x_j} \quad (3.1.9)$$

Using (3.1.8) and making appropriate thin plate approximations, we obtain from Eq. (3.1.9),

$$\left. \begin{aligned} E_{11} &= \varepsilon_1 - \kappa_1 x_3 \\ E_{22} &= \varepsilon_2 - \kappa_2 x_3 \\ E_{12} &= \varepsilon_{12} - \kappa_{12} x_3 \end{aligned} \right\} (3.1.10)$$

where ε_1 , ε_2 , ε_{12} are middle surface strain components and κ_1 , κ_2 , κ_{12} middle surface curvature components.

$$\left. \begin{aligned} \varepsilon_1 &= \frac{\partial U_1}{\partial x_1} + \frac{1}{2} \left(\frac{\partial w}{\partial x_1} \right)^2 \\ \varepsilon_2 &= \frac{\partial U_2}{\partial x_2} + \frac{1}{2} \left(\frac{\partial w}{\partial x_2} \right)^2 \end{aligned} \right\} (3.1.11)$$

$$\kappa_1 = \frac{\partial^2 w}{\partial x_1^2}, \quad \kappa_2 = \frac{\partial^2 w}{\partial x_2^2}, \quad \kappa_{12} = \frac{\partial^2 w}{\partial x_1 \partial x_2} \quad (3.1.12)$$

We assume that strain energy Π is a function of E_{11} , E_{22} , and E_{12}

$$\Pi = \Pi(E_{11}, E_{22}, E_{12}) \quad (3.1.13)$$

With (3.1.10), we see that the plate strain energy density is a function of ε_1 , ε_2 , ε_{12} , κ_1 , κ_2 , κ_{12} .

$$\dot{\Sigma} = \dot{\Sigma}(\varepsilon_1, \varepsilon_2, \varepsilon_{12}; \kappa_1, \kappa_2, \kappa_{12}) \quad (3.1.14)$$

With form (3.1.14) and (3.1.8), the work energy principle (3.1.7) yields:

$$\begin{aligned}
 & \left(\frac{\partial \Sigma}{\partial \varepsilon_1} - N_{11} \right) \frac{\partial \dot{U}_1}{\partial x_1} + \left(\frac{\partial \Sigma}{\partial \varepsilon_2} - N_{22} \right) \frac{\partial \dot{U}_2}{\partial x_2} \\
 & + \left(\frac{1}{2} \frac{\partial \Sigma}{\partial \varepsilon_{12}} - N_{21} \right) \frac{\partial \dot{U}_1}{\partial x_2} + \left(\frac{1}{2} \frac{\partial \Sigma}{\partial \varepsilon_{12}} - N_{12} \right) \frac{\partial \dot{U}_2}{\partial x_1} \\
 & + \left(\frac{\partial \Sigma}{\partial \varepsilon_1} \frac{\partial w}{\partial x_1} + \frac{1}{2} \frac{\partial \Sigma}{\partial \varepsilon_{12}} \frac{\partial w}{\partial x_2} + N_{31} - N_{13} \right) \frac{\partial w}{\partial x_1} \\
 & + \left(\frac{\partial \Sigma}{\partial \varepsilon_2} \frac{\partial w}{\partial x_2} + \frac{1}{2} \frac{\partial \Sigma}{\partial \varepsilon_{12}} \frac{\partial w}{\partial x_1} - N_{23} + N_{32} \right) \frac{\partial w}{\partial x_2} \\
 & + \left(\frac{\partial \Sigma}{\partial \kappa_1} + M_{11} \right) \frac{\partial^2 w}{\partial x_1^2} + \left(\frac{\partial \Sigma}{\partial \kappa_2} + M_{22} \right) \frac{\partial^2 w}{\partial x_2^2} \\
 & + \left(\frac{\partial \Sigma}{\partial \kappa_{12}} + M_{12} + M_{21} \right) \frac{\partial^2 w}{\partial x_1 \partial x_2} = 0
 \end{aligned} \tag{3.1.15}$$

Assuming the rates in (3.1.15) are independent and arbitrary, we obtain the stress-strain relations:

$$\left. \begin{aligned} N_{11} &= \frac{\partial \dot{z}}{\partial \epsilon_1}, & N_{22} &= \frac{\partial \dot{z}}{\partial \epsilon_2} \\ N_{12} &= N_{21} = \frac{1}{2} \frac{\partial \dot{z}}{\partial \epsilon_{12}} \end{aligned} \right\} (3.1.16)$$

$$\left. \begin{aligned} N_{13} &= N_{31} + N_{11} \frac{\partial w}{\partial x_1} + N_{12} \frac{\partial w}{\partial x_2} \\ N_{23} &= N_{32} + N_{22} \frac{\partial w}{\partial x_2} + N_{21} \frac{\partial w}{\partial x_1} \end{aligned} \right\} (3.1.17)$$

$$\left. \begin{aligned} M_{11} &= - \frac{\partial \dot{z}}{\partial \kappa_1}, & M_{22} &= - \frac{\partial \dot{z}}{\partial \kappa_2} \\ M_{12} + M_{21} &= - \frac{\partial \dot{z}}{\partial \kappa_{12}} \end{aligned} \right\} (3.1.18)$$

Eqs. (3.1.4), (3.1.5), (3.1.11), (3.1.12), (3.1.16), (3.1.17), and (3.1.18) are a basic set of equations governing the large deformation of anisotropic plates. For future use, we next combine some of these equations. From (3.1.5) and (3.1.17) we obtain:

$$\left. \begin{aligned} N_{13} &= \frac{\partial M_{11}}{\partial x_1} + \frac{\partial M_{21}}{\partial x_2} + N_{11} \frac{\partial w}{\partial x_1} + N_{12} \frac{\partial w}{\partial x_2} \\ N_{23} &= \frac{\partial M_{12}}{\partial x_1} + \frac{\partial M_{22}}{\partial x_2} + N_{22} \frac{\partial w}{\partial x_2} + N_{21} \frac{\partial w}{\partial x_1} \end{aligned} \right\} (3.1.19)$$

Substitute from (3.1.19) in (3.1.4)₃ to obtain:

$$\begin{aligned} & \frac{\partial^2 M_{11}}{\partial x_1^2} + \frac{\partial^2 M_{22}}{\partial x_2^2} + \frac{\partial^2 (M_{12} + M_{21})}{\partial x_1 \partial x_2} \\ & + \frac{\partial}{\partial x_1} (N_{11} \frac{\partial w}{\partial x_1} + N_{12} \frac{\partial w}{\partial x_2}) + \frac{\partial}{\partial x_2} (N_{22} \frac{\partial w}{\partial x_2} + N_{21} \frac{\partial w}{\partial x_1}) + q = 0 \end{aligned} \quad (3.1.20)$$

We next make an appropriate plate approximation to eq. (3.1.13) by expanding in a Taylor series in x_3 about $x_3 = 0$ and keeping the leading terms. Use of (3.1.10) yields:

$$H = H(\varepsilon_1, \varepsilon_2, \varepsilon_{12}) + \left. \frac{\partial H}{\partial x_3} \right|_0 x_3 + \frac{1}{2} \left. \frac{\partial^2 H}{\partial x_3^2} \right|_0 x_3^2 \quad (3.1.21)$$

With (3.1.21), the plate strain energy density $\Sigma = \int H dx_3$ becomes

$$\Sigma = h H(\varepsilon_1, \varepsilon_2, \varepsilon_{12}) + \frac{1}{24} h^3 \left. \frac{\partial^2 H}{\partial x_3^2} \right|_0 \quad (3.1.22)$$

Use of (3.1.10) and a chain rule yields:

$$\begin{aligned} \left. \frac{\partial^2 H}{\partial x_3^2} \right|_0 &= H_{11} \kappa_1^2 + H_{22} \kappa_2^2 + H_{33} \kappa_{12}^2 \\ &+ 2H_{12} \kappa_1 \kappa_2 + 2H_{13} \kappa_1 \kappa_{12} + 2H_{23} \kappa_2 \kappa_{12} \end{aligned} \quad (3.1.23)$$

where

$$H_{11} = \frac{\partial^2 H}{\partial \varepsilon_1^2}, \quad H_{12} = \frac{\partial^2 H}{\partial \varepsilon_1 \partial \varepsilon_2}, \quad \text{etc.} \quad (3.1.24)$$

With (3.1.22) and (3.1.23), (3.1.16) and (3.1.18) yield

$$\left. \begin{aligned} N_{11} &= h \frac{\partial H}{\partial \varepsilon_1} + \frac{1}{24} h^3 \left\{ \frac{\partial H_{11}}{\partial \varepsilon_1} \kappa_1^2 + \frac{\partial H_{22}}{\partial \varepsilon_1} \kappa_2^2 + \dots \right\} \\ N_{22} &= h \frac{\partial H}{\partial \varepsilon_2} + \frac{1}{24} h^3 \left\{ \frac{\partial H_{11}}{\partial \varepsilon_2} \kappa_1^2 + \frac{\partial H_{22}}{\partial \varepsilon_2} \kappa_2^2 + \dots \right\} \\ N_{12} = N_{21} &= \frac{1}{2} h \frac{\partial H}{\partial \varepsilon_{12}} + \frac{1}{48} h^3 \left\{ \frac{\partial H_{11}}{\partial \varepsilon_{12}} \kappa_1^2 + \dots \right\} \end{aligned} \right\} (3.1.25)$$

$$\left. \begin{aligned} M_{11} &= -\frac{1}{12} h^3 \{H_{11} \kappa_1 + H_{12} \kappa_2 + H_{13} \kappa_{12}\} \\ M_{22} &= -\frac{1}{12} h^3 \{H_{12} \kappa_1 + H_{22} \kappa_2 + H_{23} \kappa_{12}\} \\ M_{12} + M_{21} &= -\frac{1}{12} h^3 \{H_{13} \kappa_1 + H_{23} \kappa_2 + H_{33} \kappa_{12}\} \end{aligned} \right\} (3.1.26)$$

The basic equations are (3.1.4)₁, (3.1.4)₂, (3.1.11), (3.1.12), (3.1.20), (3.1.25), and (3.1.26). These are fifteen equations in fifteen variables.

For an isotropic material, H is a function of the invariants of the strain tensor.

$$H = H(I, II); \quad I = \varepsilon_1 + \varepsilon_2, \quad II = \varepsilon_1 \varepsilon_2 - \varepsilon_{12}^2 \quad (3.1.27)$$

Linear isotropic elasticity corresponds to the functional form:

$$H = \frac{E}{2(1-\nu^2)} I^2 - \frac{E}{1+\nu} II \quad (3.1.28)$$

where E is Young's modulus and ν Poisson's ratio. From eq. (3.1.28)

$$\left. \begin{aligned} \frac{\partial H}{\partial \varepsilon_1} &= \frac{E}{1-\nu^2} (\varepsilon_1 + \nu \varepsilon_2) \\ \frac{\partial H}{\partial \varepsilon_2} &= \frac{E}{1-\nu^2} (\varepsilon_2 + \nu \varepsilon_1) \\ \frac{\partial H}{\partial \varepsilon_{12}} &= \frac{2E}{1+\nu} \varepsilon_{12} \end{aligned} \right\} (3.1.29)$$

$$\left. \begin{aligned} H_{11} = H_{22} &= \frac{E}{1-\nu^2}, \quad H_{13} = H_{23} = 0 \\ H_{12} &= \frac{\nu E}{1-\nu^2}, \quad H_{33} = \frac{2E}{1+\nu} \end{aligned} \right\} (3.1.30)$$

Eqs. (3.1.25) and (3.1.26) become

$$\left. \begin{aligned} N_{11} &= \frac{hE}{1-\nu^2} (\varepsilon_1 + \nu \varepsilon_2) \\ N_{22} &= \frac{hE}{1-\nu^2} (\nu \varepsilon_1 + \varepsilon_2) \\ N_{12} = N_{21} &= \frac{hE}{1+\nu} \varepsilon_{12} \end{aligned} \right\} (3.1.31)$$

$$\begin{aligned}
M_{11} &= - \frac{Eh^3}{12(1-\nu^2)} (\kappa_1 + \nu\kappa_2) \\
M_{22} &= - \frac{Eh^3}{12(1-\nu^2)} (\nu\kappa_1 + \kappa_2) \\
M_{12} + M_{21} &= - \frac{Eh^3}{6(1+\nu)} \kappa_{12}
\end{aligned}
\quad \left. \vphantom{\begin{aligned} M_{11} \\ M_{22} \\ M_{12} + M_{21} \end{aligned}} \right\} (3.1.32)$$

For a linear orthotropic material the strain energy function takes the form

$$\begin{aligned}
H &= \frac{E_1}{2(1-\nu_1\nu_2)} (\varepsilon_1^2 + \nu_2 \varepsilon_1 \varepsilon_2) \\
&+ \frac{E_2}{2(1-\nu_1\nu_2)} (\varepsilon_2^2 + \nu_1 \varepsilon_1 \varepsilon_2) + G \varepsilon_{12}^2
\end{aligned}
\quad (3.1.33)$$

where $\nu_2 E_1 = \nu_1 E_2$.

We obtain

$$\begin{aligned}
\frac{\partial H}{\partial \varepsilon_1} &= \frac{E_1}{1-\nu_1\nu_2} (\varepsilon_1 + \nu_2 \varepsilon_2) \\
\frac{\partial H}{\partial \varepsilon_2} &= \frac{E_2}{1-\nu_1\nu_2} (\nu_1 \varepsilon_1 + \varepsilon_2) \quad , \quad \frac{\partial H}{\partial \varepsilon_{12}} = 2G\varepsilon_{12}
\end{aligned}
\quad \left. \vphantom{\begin{aligned} \frac{\partial H}{\partial \varepsilon_1} \\ \frac{\partial H}{\partial \varepsilon_2} \end{aligned}} \right\} (3.1.34)$$

$$\begin{aligned}
H_{11} &= \frac{E_1}{1-\nu_1\nu_2} \quad , \quad H_{22} = \frac{E_2}{1-\nu_1\nu_2} \\
H_{12} = H_{21} &= \frac{\nu_2 E_1}{1-\nu_1\nu_2} \quad , \quad H_{13} = H_{23} = 0 \quad , \quad H_{33} = 2G
\end{aligned}
\quad \left. \vphantom{\begin{aligned} H_{11} \\ H_{22} \\ H_{12} = H_{21} \end{aligned}} \right\} (3.1.35)$$

Eqs. (3.1.25) and (3.1.26) become

$$\left. \begin{aligned} N_{11} &= \frac{hE_1}{1-\nu_1\nu_2} (\varepsilon_1 + \nu_2\varepsilon_2) \\ N_{22} &= \frac{hE_2}{1-\nu_1\nu_2} (\nu_1\varepsilon_1 + \varepsilon_2), \quad N_{12} = 2Gh\varepsilon_{12} \end{aligned} \right\} (3.1.36)$$

$$\left. \begin{aligned} M_{11} &= -\frac{E_1 h^3}{12(1-\nu_1\nu_2)} (\kappa_1 + \nu_2\kappa_2) \\ M_{22} &= -\frac{E_2 h^3}{12(1-\nu_1\nu_2)} (\nu_1\kappa_1 + \kappa_2) \\ M_{12} + M_{21} &= -\frac{h^3 G}{6} \kappa_{12} \end{aligned} \right\} (3.1.37)$$

A Small Perturbation Stability Theory

Assume that the prebuckled deformation is homogeneous and involves no bending. that is, ε_1 , ε_2 , ε_{12} , w , N_{11} , N_{22} , and N_{12} are constant. The governing equations of the prebuckled deformation are:

$$\left. \begin{aligned} \varepsilon_1 &= \frac{\partial u_1}{\partial x_1}, \quad \varepsilon_2 = \frac{\partial u_2}{\partial x_2}, \quad \varepsilon_{12} = \frac{1}{2} \left(\frac{\partial u_1}{\partial x_2} + \frac{\partial u_2}{\partial x_1} \right) \\ N_{11} &= h \frac{\partial H}{\partial \varepsilon_1}, \quad N_{22} = h \frac{\partial H}{\partial \varepsilon_2}, \quad N_{12} = N_{21} = \frac{1}{2} h \frac{\partial H}{\partial \varepsilon_{12}} \end{aligned} \right\} (3.2.1)$$

These variables are perturbed by additional quantities at buckling which are assumed to be small and the equations linearized accordingly. We shall not write down all the equations governing the perturbation but just consider what happens to eq. (3.1.20). It becomes, with $q = 0$,

$$\begin{aligned}
& \frac{\partial^2 M_{11}}{\partial x_1^2} + \frac{\partial^2 M_{22}}{\partial x_2^2} + \frac{\partial^2 (M_{12} + M_{21})}{\partial x_1 \partial x_2} \\
& + N_{11} \frac{\partial^2 w}{\partial x_1^2} + 2N_{12} \frac{\partial^2 w}{\partial x_1 \partial x_2} + N_{22} \frac{\partial^2 w}{\partial x_2^2} = 0 \quad (3.2.2)
\end{aligned}$$

Use (3.1.12) and (3.1.26) to write the moments in (3.2.2) in terms of buckled displacement w .

$$\begin{aligned}
& \frac{h^3}{12} H_{11} \frac{\partial^4 w}{\partial x_1^4} + H_{22} \frac{\partial^4 w}{\partial x_2^4} + (2H_{12} + H_{33}) \frac{\partial^4 w}{\partial x_1^2 \partial x_2^2} \\
& + 2H_{13} \frac{\partial^4 w}{\partial x_1^3 \partial x_2} + 2H_{23} \frac{\partial^4 w}{\partial x_1 \partial x_2^3} \\
& = N_{11} \frac{\partial^2 w}{\partial x_1^2} + 2N_{12} \frac{\partial^2 w}{\partial x_1 \partial x_2} + N_{22} \frac{\partial^2 w}{\partial x_2^2} \quad (3.2.3)
\end{aligned}$$

In this equation, w is the displacement due to buckling, while N_{11} , N_{12} , and N_{22} are associated with the prebuckled deformation. H_{ij} are functions of ε_1 , ε_2 , and ε_{12} associated with the prebuckled deformation.

For the linear isotropic material, the H_{ij} are given by (3.1.30) and (3.2.3) becomes

$$\frac{Eh^3}{12(1-\nu^2)} \nabla^2 \nabla^2 w = N_{11} \frac{\partial^2 w}{\partial x_1^2} + 2N_{12} \frac{\partial^2 w}{\partial x_1 \partial x_2} + N_{22} \frac{\partial^2 w}{\partial x_2^2} \quad (3.2.4)$$

where $\nabla^2 w = \partial^2 w / \partial x_1^2 + \partial^2 w / \partial x_2^2$.

For the linear orthotropic material, the H_{ij} are given by (3.1.35) and eq. (3.2.3) becomes

$$\begin{aligned}
 & D_1 \frac{\partial^4 w}{\partial x_1^4} + 2(D'+C) \frac{\partial^4 w}{\partial x_1^2 \partial x_2^2} + D_2 \frac{\partial^4 w}{\partial x_2^4} \\
 & = N_{11} \frac{\partial^2 w}{\partial x_1^2} + 2N_{12} \frac{\partial^2 w}{\partial x_1 \partial x_2} + N_{22} \frac{\partial^2 w}{\partial x_2^2}
 \end{aligned} \tag{3.2.5}$$

where

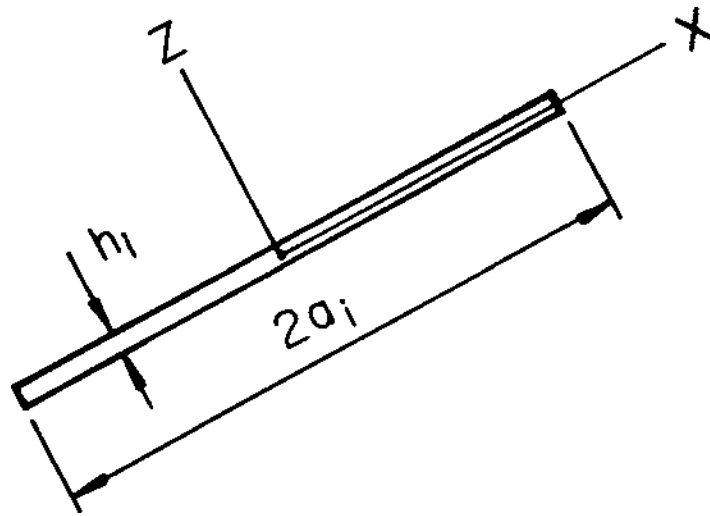
$$\begin{aligned}
 D_1 &= \frac{E_1 h^3}{12(1-\nu_1 \nu_2)}, & D_2 &= \frac{E_2 h^3}{12(1-\nu_1 \nu_2)} \\
 D' &= \nu_2 D_1 = \nu_1 D_2, & C &= \frac{h^3 G}{12}
 \end{aligned} \tag{3.2.6}$$

Note (3.1.37) can be written

$$\begin{aligned}
 M_{11} &= -D_1(\kappa_1 + \nu_2 \kappa_2) \\
 M_{22} &= -D_2(\nu_1 \kappa_1 + \kappa_2) \\
 M_{12} + M_{21} &= -2C\kappa_{12}
 \end{aligned} \tag{3.2.7}$$

Local Instability of Corrugated Fiberboard

The preceding stability theory is applied to the buckling of corrugated fiberboard subject to axial compression. As modeled (fig. 1), it is a periodic structure of three rigidly connected plate elements, with thicknesses h_i and widths $2a_i$. Local coordinates are chosen for each plate element with the origin at the center (fig. 8). Let the prebuckled loading be an axial strain ϵ in each plate in the y-direction. If the Poisson's ratios of the material of each plate are equal, their strains in the x-direction will be the same. Hence, the plates will deform without bending and form a figure which is geometrically similar to the



M 148 080

Figure 8.--Local coordinates for plate elements of model.

undeformed figure. We assume that the prebuckled deformation has this feature even though the deformations are large enough to necessitate use of a tangent modulus theory. Under this assumption the prebuckled deformation is homogeneous so that the equations of the preceding section can be used for each plate element.

We now make two assumptions. We assume that each element of the model can be treated as an isotropic plate and use eq. (3.2.4). Because it is found that buckling takes place at strains beyond the linear elastic limit, we account for this by using the tangent modulus for E. E is therefore a function of the strain ϵ . It is the cross-machine modulus of the paper. Paper, of course, is highly anisotropic so that a more accurate theory would use (3.2.5) rather than (3.2.4). The magnitude of the error in this approximation remains to be investigated. Also, the tangent modulus assumption which is ad hoc should be justified by showing that there is a strain energy density \bar{H} which leads to eqs. (3.1.30) with constant E replaced by the tangent modulus $E(\epsilon)$.

For axial compression, $N_{12} = N_{11} = 0$, $N_{22} = N$ and eq. (3.2.4) becomes

$$\nabla^2 \nabla^2 w + \frac{12(1-\nu^2)N}{Eh^3} \frac{\partial^2 w}{\partial y^2} = 0 \quad (3.3.1)$$

The buckling load N is the smallest eigenvalue for which eq. (3.3.1) has a non-trivial solution. The buckling modes are assumed to take the following separated form:

$$w = f(x) \sin(\lambda_n y) \quad , \quad \lambda_n = \frac{n\pi}{L} \quad (3.3.2)$$

which corresponds to taking the edges of the plate elements simply supported at $y = 0, L$. Substituting (3.3.2) in (3.3.1) yields the following equation for $f(x)$:

$$\left(\frac{d^2}{dx^2} - \lambda_n^2 \right)^2 f - \frac{12(1-\nu^2)N}{Eh^3} \lambda_n^2 f = 0 \quad (3.3.3)$$

The general solution of (3.3.3) is

$$f(x) = c_1 \cosh(\alpha_1 x) + c_2 \cosh(\alpha_2 x) + c_3 \sinh(\alpha_1 x) + c_4 \sinh(\alpha_2 x) \quad (3.3.4)$$

where

$$\begin{Bmatrix} \alpha_1 \\ \alpha_2 \end{Bmatrix} = \lambda_n \sqrt{1 \pm \frac{\sqrt{12(1-\nu^2)}N}{\lambda_n^2 E h^3}} \quad (3.3.5)$$

The primary buckling mode is even in x in each plate element (fig. 4). Hence, $c_3 = c_4 = 0$ in solution (3.3.4) and c_1 and c_2 are to be determined from appropriate boundary conditions. The solution in each plate element is

$$f_i(x) = c_{i1} \cosh(\alpha_{i1} x) + c_{i2} \cosh(\alpha_{i2} x) \quad (3.3.6)$$

where index i denotes the element and

$$\begin{Bmatrix} \alpha_{i1} \\ \alpha_{i2} \end{Bmatrix} = \lambda_n \sqrt{1 \pm \frac{\sqrt{12(1-\nu_i^2)}N_i}{\lambda_n^2 E_i h_i^3}} \quad (3.3.7)$$

For boundary conditions we require zero deflections at the junction of plate elements,

$$w_1(a_1) = w_2(-a_2) = w_3(-a_3) = 0 \quad (3.3.8)$$

equal rotation of each element at junctions,

$$\frac{\partial w_1(a_1)}{\partial x} = \frac{\partial w_2(-a_2)}{\partial x} = \frac{\partial w_3(-a_3)}{\partial x} = R \sin(\lambda_n y) \quad (3.3.9)$$

and moment equilibrium at junctions,

$$M_{1x}(a_1) - M_{2x}(-a_2) - M_{3x}(-a_3) = 0 \quad (3.3.10)$$

Conditions (3.3.8) are approximations to the more accurate conditions that would require equal deflection of elements at junctions. Conditions (3.3.8) result from assuming that in-plane buckling displacements in each plate element are negligible compared to transverse displacements w_i . Because of this assumption it is not possible to impose force equilibrium at each joint. This assumption has been made and justified for aircraft structures (1).

Eqs. (3.3.8) yield

$$c_{i1} = -c_{i1} \frac{\cosh(\alpha_{i2} a_1)}{\cosh(\alpha_{i1} a_1)} \quad (3.3.11)$$

while (3.3.9) and (3.3.11) combine to give

$$c_{12} = \frac{R \cosh(\alpha_{11} a_1)}{\alpha_{12} \cosh(\alpha_{11} a_1) \sinh(\alpha_{12} a_1) - \alpha_{11} \cosh(\alpha_{12} a_1) \sinh(\alpha_{11} a_1)} \quad (3.3.12)$$

with similar expressions for c_{22} and c_{32} . Using (3.1.32), (3.3.11), and (3.3.12) yields:

$$M_{1x}(a_1) = - \frac{E_1 h_1^3}{12(1-\nu_1^2)} \frac{(\alpha_{11}^2 - \alpha_{12}^2) R \sin(\lambda_n y)}{\alpha_{11} \tanh(\alpha_{11} a_1) - \alpha_{12} \tanh(\alpha_{12} a_1)}$$

with similar expressions for $M_{2x}(-a_2)$ and $M_{3x}(-a_3)$. The moment equilibrium equation (3.3.10) yields the buckling equation:

$$K_1 + K_2 + K_3 = 0 \quad (3.3.13)$$

where the K_i ($i = 1, 2, 3$) are plate element stiffness coefficients.

$$K_i = \frac{E_i h_i^2 \sqrt{N_i/E_i h_i (1-v_i^2)}}{-L^3 \alpha_{i2} \tanh(\alpha_{i2} a_i) + L^3 \alpha_{i1} \tanh(\alpha_{i1} a_i)} \quad (3.3.14)$$

Write

$$\begin{aligned} \sigma_i &= N_i/h_i, \quad t_i = h_i/L, \quad b_i = a_i/L \\ \alpha_i = \sqrt{-1} L \alpha_{i2} &= n\pi \sqrt{\frac{\sqrt{12(1-v_i^2)} \sigma_i/E_i}{n\pi t_i} - 1} \\ \beta_i = L \alpha_{i1} &= n\pi \sqrt{\frac{\sqrt{12(1-v_i^2)} \sigma_i/E_i}{n\pi t_i} + 1} \end{aligned} \quad (3.3.15)$$

Then the stiffness coefficients can be written in the form

$$K_i = \frac{E_i t_i^2 \sqrt{(1-v_i^2)} \sigma_i/E_i}{\alpha_i \tanh(\alpha_i b_i) + \beta_i \tanh(\beta_i b_i)} \quad (3.3.16)$$

Because σ_i and E_i are functions of the axial strain ϵ , eq. (3.3.13) is an equation for the buckling strain E on the structure. Its solution is considered in the section "Buckling Model Development."

Literature Cited

1. Cox, H.L.
1954. Computation of initial buckling stress for sheet-stiffener combinations. J. Royal Aeronaut. Soc. 58:634-638.
2. Fung, Y. C.
1965. Foundations of solid mechanics. Prentice-Hall, Englewood Cliffs, N.J.
3. Jackson, C. A., J. W. Koning, Jr., and W. A. Gatz.
1976. Edgewise compressive test of paperboard by a new method. Pulp Pap. Can. 77(10):43-46.
4. Kellicutt, K. Q.
1959. Relationship of moment of inertia to stiffness of corrugated board. Package Eng. 44(10):80, 105.
5. Koning, J. W., Jr.
1978. Compressive properties of linerboard as related to corrugated fiberboard containers: theoretical model verification. Tappi 61(8):69.
6. Koning, J. W., Jr., and W. D. Godshall.
1975. Repeated recycling of corrugated containers and its effect on strength properties. Tappi 58(9):146.
7. McKee, R. C., J. W. Gander, and J. R. Wachuta
1963. Compression strength formula for corrugated boxes. Paperboard Packag. Rep. 79. Inst. Pap. Chem., Appleton, Wis.
8. Moody, R. C.
1965. Edgewise compression strength of corrugated fiberboard as determined by local instability U.S. For. Serv. Res. Pap. FPL 46. For. Prod. Lab., Madison, Wis.
9. Moody, R. C., and J. W. Koning, Jr.
1966. Effect of load rate on the edgewise compressive strength of corrugated fiberboard. U.S. For. Serv. Res. Note FPL 0121. For. Prod. Lab., Madison, Wis.
10. Setterholm, V. C.
1974. A new concept in paper thickness measurement. Tappi 57(3):164.
11. Technical Association of the Pulp and Paper Industry
1970. T811. Tappi 53(7):1379.
12. Zahn, J. J.
1973. Local buckling of orthotropic truss-core sandwich. USDA For. Serv. Res. Pap. FPL 220. For. Prod. Lab., Madison, Wis.

